

## PLANT SCIENCES

# Mechanism of mixed-linkage glucan biosynthesis by barley cellulose synthase–like CslF6 (1,3;1,4)- $\beta$ -glucan synthase

Pallinti Purushotham<sup>1,2</sup>, Ruoya Ho<sup>1,2</sup>, Long Yu<sup>3,4</sup>, Geoffrey B. Fincher<sup>4</sup>, Vincent Bulone<sup>3,4,5†</sup>, Jochen Zimmer<sup>1,2\*</sup>

Mixed-linkage (1,3;1,4)- $\beta$ -glucans, which are widely distributed in cell walls of the grasses, are linear glucose polymers containing predominantly (1,4)- $\beta$ -linked glucosyl units interspersed with single (1,3)- $\beta$ -linked glucosyl units. Their distribution in cereal grains and unique structures are important determinants of dietary fibers that are beneficial to human health. We demonstrate that the barley cellulose synthase-like CslF6 enzyme is sufficient to synthesize a high-molecular weight (1,3;1,4)- $\beta$ -glucan in vitro. Biochemical and cryo-electron microscopy analyses suggest that CslF6 functions as a monomer. A conserved “switch motif” at the entrance of the enzyme’s transmembrane channel is critical to generate (1,3)-linkages. There, a single-point mutation markedly reduces (1,3)-linkage formation, resulting in the synthesis of cellulosic polysaccharides. Our results suggest that CslF6 monitors the orientation of the nascent polysaccharide’s second or third glucosyl unit. Register-dependent interactions with these glucosyl residues reposition the polymer’s terminal glucosyl unit to form either a (1,3)- or (1,4)- $\beta$ -linkage.

## INTRODUCTION

Cell walls are dynamic carbohydrate-rich extracellular matrices present in most phyla. They define cell shape, mediate tissue organization and organismal growth, and provide resilience to adverse environmental stresses. In the cell walls of terrestrial plants, cellulose forms a load-bearing network of microfibrils that are embedded in a complex composite of hemicelluloses, pectins, proteins, and, in specific tissues, lignins (1).

Mixed-linkage (1,3;1,4)- $\beta$ -glucans are abundant polymers of cell walls of the Poaceae (i.e., grasses) and are generally absent in the walls of eudicots (2). The (1,3;1,4)- $\beta$ -glucans of common cereal species consist of ~25 and ~75% of (1,3)- and (1,4)- $\beta$ -linked glucosyl units, respectively, in an unbranched and unsubstituted polymer. The structure of the polysaccharide consists largely of cellotriosyl and cellotetraosyl units separated by single (1,3)- $\beta$ -linkages (2). The (1,3)-linkages introduce flexible kinks at irregular intervals into the polysaccharide (2, 3). As a result, (1,3;1,4)- $\beta$ -glucans do not easily align to form insoluble fibers, as is observed with the (1,4)- $\beta$ -glucan produced by cellulose synthase (CesA). Because of their increased water solubility, (1,3;1,4)- $\beta$ -glucans form highly viscous aqueous solutions. These properties provide important benefits in human health by reducing the risk of serious diseases, including colorectal cancer, type 2 diabetes, and coronary heart disease (4, 5).

The variability of (1,3;1,4)- $\beta$ -glucan structures can be expressed in terms of their DP3:DP4 ratios, where DP is the degree of

polymerization and DP3 and DP4 are easily measurable indicators of cellotriosyl and cellotetraosyl units, respectively (6). The DP3 and DP4 fragments are released upon degradation with lichenase, which is an endo-(1,3;1,4)- $\beta$ -glucanase that hydrolyzes the (1,4)- $\beta$ -linkage directly following, toward the reducing end of the polysaccharide, a (1,3)- $\beta$ -linked glucosyl unit (7). Water-soluble (1,3;1,4)- $\beta$ -glucans generally have DP3:DP4 ratios of about 2:1 to 3:1.

A major class of enzymes involved in the formation of plant cell wall polysaccharides is family 2 glycosyltransferases (GTs), including CesAs (8). The CesA enzyme couples cellulose synthesis with polysaccharide secretion through a transmembrane (TM) channel formed by its membrane-embedded region. The enzyme uses uridine diphosphate (UDP)-glucose as a substrate and elongates and translocates the nascent cellulose polymer one glucosyl unit at a time (9). In the SN<sub>2</sub>-like substitution reaction (10), the C4 hydroxyl of cellulose’s nonreducing end glucosyl unit (the acceptor) mediates a nucleophilic attack on the C1 carbon of the substrate’s glucosyl residue (the donor). This reaction is facilitated by a base catalyst that deprotonates the acceptor during the nucleophilic attack (10). The base catalyst is formed by the aspartate residue of an invariant Thr-Glu-Asp (TED) motif of the active site that is in hydrogen bond distance to the acceptor’s C4 hydroxyl (9).

The enzymes involved in (1,3;1,4)- $\beta$ -glucan formation in grasses most likely use a similar reaction mechanism. They belong to the CesA-like CslF, CslH, and CslJ groups of enzymes (11–13). Among those, the CslF6 enzyme, which is the predominant isoenzyme in developing barley grain, is closely related to CesAs, as reflected in a high degree of sequence similarity across the catalytic domains and TM regions, as well as similar predicted TM topologies (8, 14, 15). Specifically, the CslF clade is nested within the CslD subfamily and evolved following the CesA-CslD divergence (11, 16). Although the functions of all CslD enzymes have not been defined unequivocally, some have been implicated in cellulose formation in tip-growing cells (13, 17, 18).

The similarity of (1,3;1,4)- $\beta$ -glucan synthases with CesA and the unusual and variable structural features of (1,3;1,4)- $\beta$ -glucans raise

Copyright © 2022 The Authors, some rights reserved; exclusive licensee American Association for the Advancement of Science. No claim to original U.S. Government Works. Distributed under a Creative Commons Attribution NonCommercial License 4.0 (CC BY-NC).

<sup>1</sup>Howard Hughes Medical Institute, University of Virginia School of Medicine, Charlottesville, VA 22908, USA. <sup>2</sup>Department of Molecular Physiology and Biological Physics, University of Virginia School of Medicine, 480 Ray C. Hunt Dr., Charlottesville, VA 22908, USA <sup>3</sup>Adelaide Glycomics, University of Adelaide, Waite Campus, Glen Osmond, SA 5064, Australia. <sup>4</sup>School of Agriculture, Food, and Wine, University of Adelaide, Waite Campus, Glen Osmond, SA 5064, Australia. <sup>5</sup>Division of Glycoscience, Department of Chemistry, School of Engineering Sciences in Chemistry, Biotechnology, and Health, Royal Institute of Technology (KTH), AlbaNova University Centre, Stockholm, SE-10691, Sweden.

\*Corresponding author. Email: jz3x@virginia.edu

†Present address: College of Medicine and Public Health, Health Sciences Building, Flinders University, Bedford Park Campus, Sturt Road, South Australia 5042, Australia.

two important, unanswered questions about their biosynthesis. First, can both linkage types be inserted into the polysaccharide by a single enzyme, or are multiple enzymes required (19–21)? Second, how does the enzyme or enzyme complex nonrandomly incorporate single (1,3)- $\beta$ -linkages into a (1,4)- $\beta$ -backbone, while the cellotriosyl and cellobiotetraosyl units between these (1,3)-linkages are arranged at random?

To shed light on these fundamental questions in cell wall polysaccharide biosynthesis, we have expressed barley (*Hordeum vulgare*) CslF6 in Sf9 insect cells to test its ability to synthesize a (1,3;1,4)- $\beta$ -glucan in the absence of other plant-derived components. Our results unambiguously demonstrate the formation of (1,3;1,4)- $\beta$ -glucans with DPs of 25 to 100 and with structures similar to (1,3;1,4)- $\beta$ -glucans isolated from barley grain. In addition, we determined a medium-resolution cryo-electron microscopy (cryo-EM) structure of the monomeric enzyme at an intermediate state during polymer biosynthesis. The structure and primary sequence analyses identified a motif at the entrance of the enzyme's TM channel that is necessary for (1,3)- $\beta$ -linkage formation and the switch in enzyme specificity.

## RESULTS

The approach established for hybrid aspen Cesa8 (22) was adapted to express and purify barley CslF6, as described in Materials and Methods. To facilitate the detection and purification of the recombinant enzyme, a polyhistidine tag was introduced at the protein's N terminus.

### CslF6 purifies as a monomeric, catalytically active species

CslF6 was extracted from the membrane fraction in a detergent mixture of lauryl maltose neopentyl glycol (LMNG) and cholesteryl hemisuccinate (CHS) and later exchanged into glyco-diosgenin (GDN) during metal affinity chromatography. The protein elutes as an essentially symmetric peak from a Superose 6 size exclusion chromatography column (Fig. 1A), although minor higher-molecular weight species are present. Although protein molecular weights are difficult to estimate in a micelle-embedded state, the observed CslF6 elution volume suggests a lower molecular weight compared to a Cesa8 homotrimer purified in the same detergent (22).

Attempts to verify the formation of a stable oligomeric complex similar to the Cesa8 trimer by copurification of coexpressed His-, Myc-, and FLAG-tagged CslF6 species failed. Only weak interactions were observed that may arise from nonspecific contacts or protein aggregation upon detergent solubilization (fig. S1, A and B). This suggests that CslF6 functions as a monomer. Accordingly, CslF6 species eluting at apparent higher and lower molecular weights from the size exclusion chromatography column (Fig. 1A) exhibit similar catalytic activities (explained below; fig. S1C). Therefore, we conclude that the small fraction of higher-molecular weight CslF6 species by size exclusion chromatography primarily arises from copurifying protein-bound polysaccharides of various lengths, as confirmed by cryo-EM (see below).

The catalytic activity of CslF6 can be monitored in vitro by either quantifying the produced glucan using a radiotracer or enzymatically detecting the released UDP (22, 23). We tested CslF6's in vitro catalytic activity by measuring incorporation of  $^3\text{H}$ -labeled glucose into the synthesized polymer. The labeled glucans were separated from unpolymerized tracers by descending paper chromatography, followed by scintillation counting, as previously described for hybrid aspen Cesa8 (23).

In vitro, CslF6 produces a glucan in the presence of magnesium cations and UDP-glucose (Fig. 1B). Catalytic activity is reduced to approximately 30% when magnesium is replaced with manganese, and no detectable product is formed in the presence of EDTA or calcium. Most products accumulate over ~90 min, and synthesis plateaus approximately 3 hours after initiation (Fig. 1C).

To test whether the synthesized product represents a polymer harboring both (1,3)- and (1,4)- $\beta$ -linked glucosyl units, we hydrolyzed the  $^3\text{H}$ -labeled polymer with enzymes that specifically degrade (1,3;1,4)- $\beta$ -glucans (a lichenase), cellulose [a (1,4)- $\beta$ -glucanase], or curdlan [a (1,3)- $\beta$ -glucanase] (Fig. 1D and fig. S1D). Incubating the in vitro synthesized polymer with *Bacillus subtilis* lichenase (24) reduces the amount of detectable polymeric product to about 20% compared to a control in the absence of hydrolase, demonstrating that the polymer is a (1,3;1,4)- $\beta$ -glucan (7). As expected, incubations with (1,3)- $\beta$ - and (1,4)- $\beta$ -glucan endohydrolases also degrade the polymer. Stretches of two or three adjacent (1,4)-linked glucosyl units are sufficiently long for degradation by (1,4)- $\beta$ -glucan endohydrolases (i.e., cellulase). Cleavage by the *Trichoderma* sp. (1,3)- $\beta$ -glucan endohydrolase also indicates the presence of (1,3)-linkages, as this enzyme is able to hydrolyze either a (1,3)- or a (1,4)- $\beta$ -linkage, provided that the target linkage is adjacent to a (1,3)- $\beta$ -linked glucosyl unit, toward the reducing terminus of the polysaccharide (7).

### Lichenase digestion releases DP3 and DP4 oligosaccharides from (1,3;1,4)- $\beta$ -glucan

Lichenase degradation of (1,3;1,4)- $\beta$ -glucans releases DP3 and DP4 fragments because of the specific cleavage of (1,4)-linkages following a (1,3)-linked glucosyl unit (9). Lichenase degradation of the in vitro CslF6-synthesized glucan produces DP3 and DP4 fragments that are indistinguishable from those released from control barley grain (1,3;1,4)- $\beta$ -glucans (Fig. 1E and fig. S2A). In both cases, the oligosaccharides elute from a TSKgel high-performance liquid chromatography (HPLC) size exclusion chromatography column at 15.4 min (DP4) and 16.1 min (DP3). Under the same conditions, cellotetraose and cellotriose standards elute at 15.2 and 16.0 min, respectively (Fig. 1E).

For comparison, we degraded commercially available barley (1,3;1,4)- $\beta$ -glucans with the lichenase, cellulase, and (1,3)- $\beta$ -glucan endohydrolase used to analyze the glucan synthesized in vitro. In this case, lichenase treatment generates the characteristic DP3 and DP4 fragments; cellulase releases primarily di- and tetrasaccharides; and (1,3)- $\beta$ -endohydrolase treatment produces DP4, DP3, and DP2 oligosaccharides (fig. S2A).

### Barley CslF6 synthesizes a polymeric (1,3;1,4)- $\beta$ -glucan

In addition to enzymatic degradation analyses, we performed glycosyl-linkage analysis to determine the type of glycosidic linkages forming the in vitro-synthesized glucan. First, linkage analysis of control barley grain glucans using the partially methylated alditol acetate (PMAA) method readily detected (1,3)- and (1,4)-linked glucosyl units at an approximate ratio of 1:2.2, consistent with previous reports (fig. S2, B to D) (21). Second, the same analysis of the in vitro CslF6-synthesized glucan revealed the presence of (1,3)- and (1,4)-linked glucosyl units at an approximate 1:2 ratio (Fig. 1F and fig. S3). On the basis of the abundance of terminal glucosyl units in the gas chromatography (GC) chromatogram, we estimate an average length of the polysaccharide of about 25 glucosyl units. Analyzing material produced from proteoliposome-reconstituted

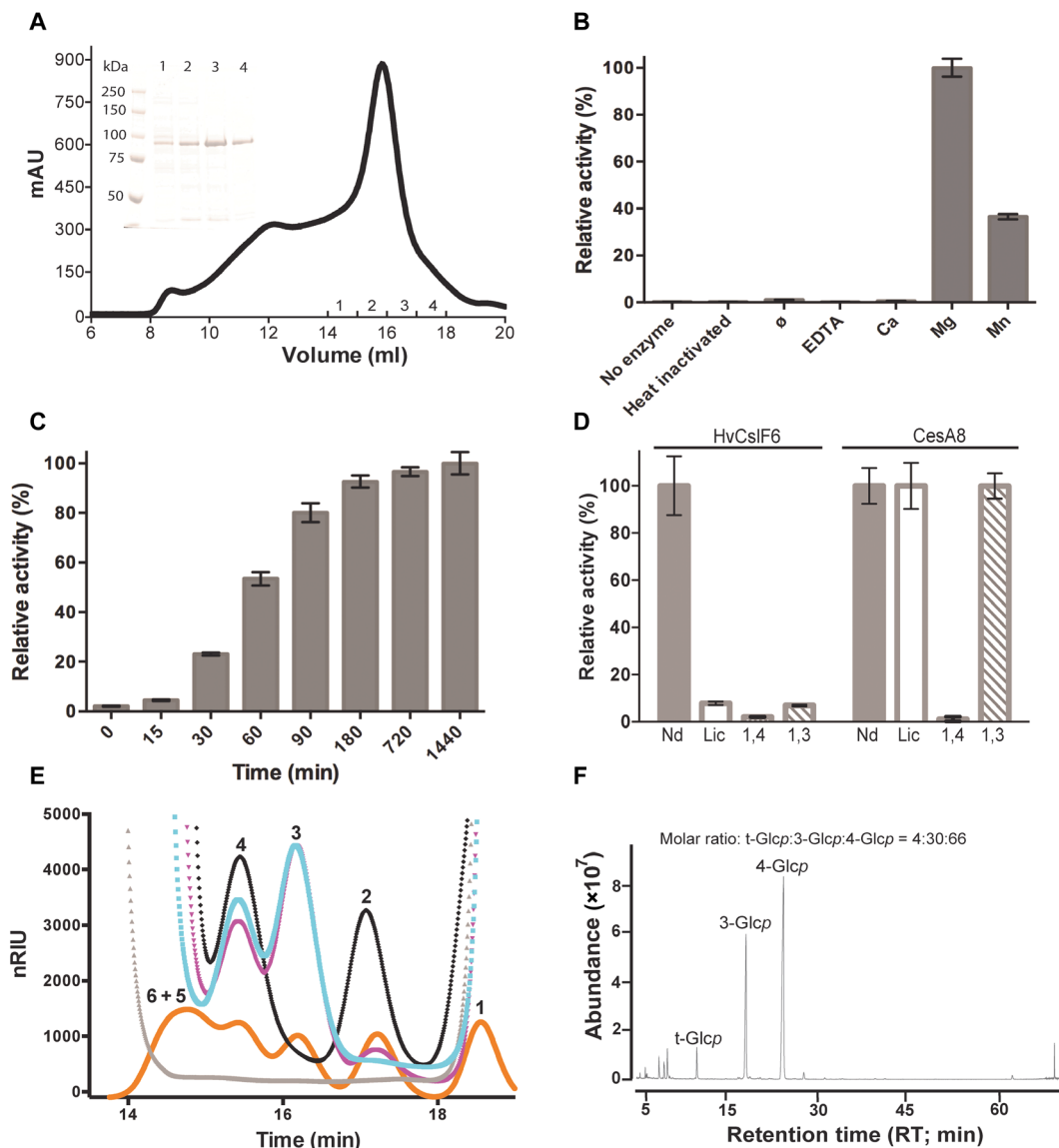


**Fig. 1. In vitro (1,3;1,4)- $\beta$ -glucan biosynthesis by barley CslF6.** (A) Size exclusion chromatography profile of GDN-solubilized CslF6. Inset: Coomassie-stained SDS-polyacrylamide gel electrophoresis (SDS-PAGE) of the indicated fractions. mAU, absorbance at 280 nm ( $\times 10^{-3}$ ). (B) Catalytic activity of purified CslF6 measured upon incorporation of  $^3\text{H}$ -labeled glucose, as described previously (23). The product yield obtained in the presence of magnesium was set to 100%. (C) Time course of product accumulation. (D) Enzymatic degradation of the in vitro-synthesized glucan. Material recovered in the absence of hydrolase was set to 100%. All error bars represent deviations from the means of at least three replicas. Nd, no digestion; Lic, lichenase; 1,4, endo-(1,4)- $\beta$ -glucanase digestion; 1,3, (1,3)- $\beta$ -glucanase digestion. (E) High-performance liquid chromatography (HPLC) size exclusion chromatography of in vitro synthesized and lichenase (cyan trace), (1,3)- $\beta$ -glucanase (magenta trace), and (1,4)- $\beta$ -glucanase (black trace) digested product. The undigested sample is shown in gray, and a standard cello-oligosaccharide mixture ranging from hexa- to monosaccharides is shown in orange (labeled 6 to 1). nRIU, nano refractive index units. (F) Glycosyl linkage analysis of the CslF6-synthesized glucan. A gas chromatogram of the separated alditol acetates is shown. The identity of the terminal, 3-, and 4-linked glucosyl units (t-Glc, 3-Glc, and 4-Glc, respectively) was confirmed by electron impact mass spectrometry (fig. S3).

CslF6, instead of detergent-solubilized enzyme, did not change the ratio of (1,3)- and (1,4)-linked glucosyl units but increased the overall polymer length to about 33 residues. Thus, our glycosidic linkage analysis independently confirms the in vitro formation of a polymeric (1,3;1,4)- $\beta$ -glucan by barley CslF6. In contrast, a linkage analysis of glucans produced by hybrid aspen CesA8, a bona fide CesA, only revealed 4-linked and terminal glucosyl units (fig. S4).

### Monomeric CslF6 adopts a CesA-like fold

Cryo-EM analyses of barley CslF6 were performed with protein species eluting from a size exclusion chromatography column at higher and lower apparent molecular weights (Fig. 1A). However, in all cases, only monomeric particles were evident from two-dimensional (2D) and 3D classifications (Fig. 2A).

Cryo-EM data processing in CryoSPARC (25) or RELION (26) generated a medium-resolution map at about  $\sim 4.0$  Å resolution that

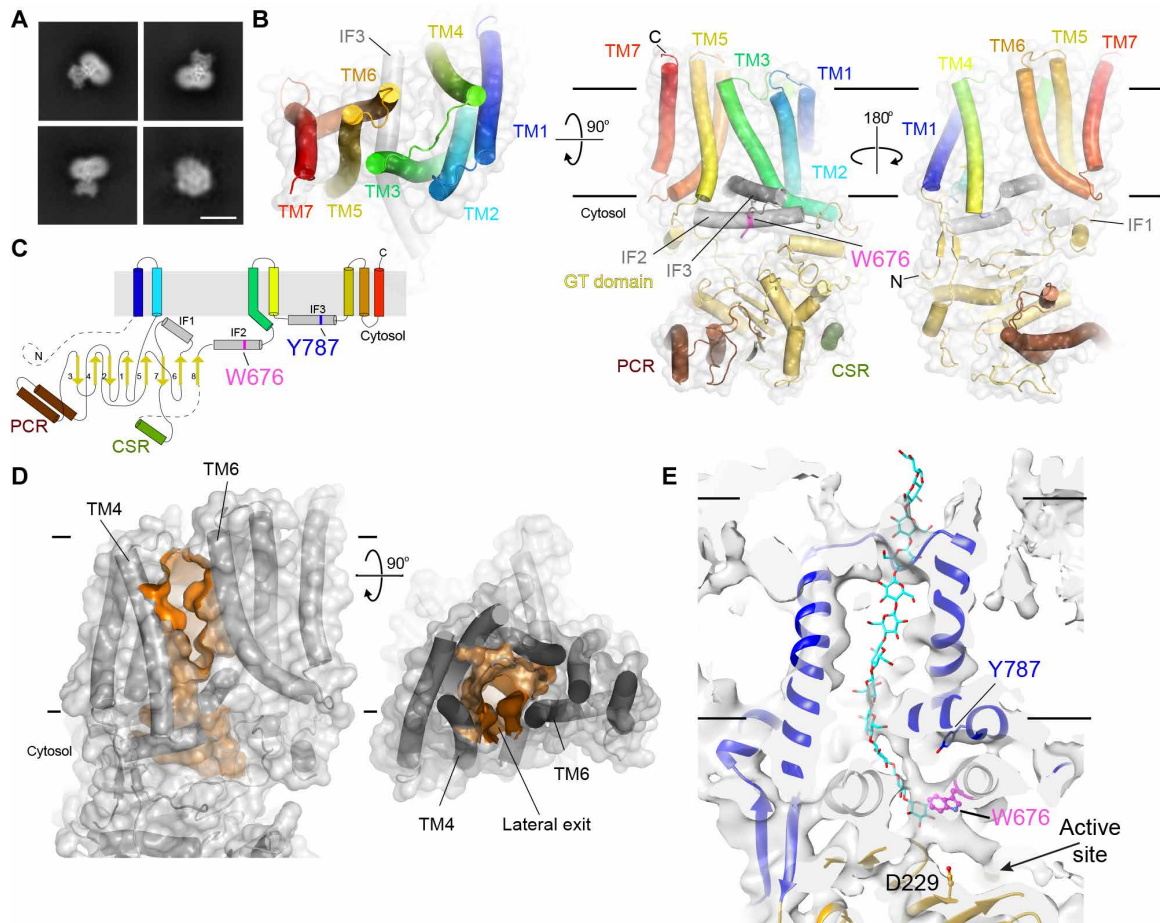


**Fig. 2. Architecture of barley CslF6.** (A) Representative 2D class averages of micelle-solubilized CslF6. Scale bar, 10 nm. (B) Cartoon representation of CslF6. TM helices are colored blue to red from the N terminus to the C terminus. The GT domain is shown in pale yellow, the plant-conserved region (PCR) and class-specific region (CSR) domains are colored brown and green, respectively. "N" and "C" denote the N and C termini of the polypeptide chain. (C) Topology diagram of CslF6 colored as in (B). (D) Monomeric CslF6 forms a TM channel with a large lateral opening. The channel was rendered using a 2.5 Å radius probe calculated in HOLLOW (37) and displayed as an orange surface. CslF6 is shown as a semitransparent surface and cartoon with cylindrical helices. Black solid lines indicate putative membrane boundaries. (E) A poorly resolved glucan likely occupies the CslF6 channel. Bacterial CesaA [Protein Data Bank (PDB): 4P00] containing an 18-residue-long nascent cellulose polymer (shown as cyan and red sticks) was overlaid with the CslF6 cryo-EM map (shown as semitransparent gray surface) to indicate the putative glucan secretion path. CslF6 is also shown as a cartoon, colored blue and pale yellow for its TM and GT domains, respectively. W676 and Y787 of the QxxRW and switch motifs are shown as sticks colored magenta and blue, respectively.

resolved all of CslF6's TM helices and most regions of its cytosolic GT domain (Fig. 2B, figs. S5 and S6, and table S1). The N-terminal 92 residues and residues 518 to 572 of the GT domain are disordered, as also observed in CesaA structures (22, 27). Building the CslF6 model took advantage of its similarity with hybrid aspen CesaA8 and a predicted AlphaFold2 model (28, 29). Therefore, the presented structure represents an AlphaFold2-generated CslF6 model refined against a medium-resolution cryo-EM map.

CslF6 contains seven TM helices with the C terminus residing on the luminal side and the catalytic domain between TM helices 2 and 3 on the cytosolic side of the membrane (Fig. 2B). TM helix 7, implicated in trimer formation in hybrid aspen CesaA8, packs against TM helices 5 and 6 at the periphery of the CslF6 core structure. The TM helices interact with three amphipathic cytosolic helices that run parallel to the membrane plane. The catalytic GT domain associates with these interface helices and protrudes into the cytosol by about 35 Å.

Compared to bacterial CesaA and other GT2 enzymes adopting a GT-A fold (30), the catalytic cores of CesaA and CslF6 contain

two insertions, referred to as plant-conserved (PCR) and class-specific (CSR) regions, respectively (31). The PCR domain, corresponding to residues 245 to 390, consists of two antiparallel  $\alpha$  helices that interact with the catalytic core on its membrane distal side, as described for CesaA (Fig. 2, B and C) (22, 32). In CesaA trimers, the PCR stabilizes a trimeric assembly by forming a triangular oligomerization domain. In CslF6, the loop connecting the two PCR helices is 15 residues longer compared to hybrid aspen CesaA8 and folds back onto the PCR helices.

The CslF6-CSR, corresponding to residues 514 to 618, is mostly disordered, as also observed in bona fide CesaA enzymes (22, 27, 33). Considering its proximity to the predicted water-lipid interface, the domain may interact with membrane lipids and/or other binding partners (Fig. 2B).

### CslF6 accommodates a nascent glucan chain inside its TM channel

CslF6 couples polysaccharide synthesis with the translocation of the polymer across the membrane. Its seven TM helices form a

continuous TM channel containing a large, likely lipid-filled, lateral opening toward the bilayer phase (Fig. 2D). At lower contour levels, a ribbon-shaped density is evident inside the TM channel, starting at the active site and spanning approximately half the channel (Fig. 2E). The shape and position of this nonproteinaceous density resembles the cellulose polymer observed in plant and bacterial CesAs (22, 27, 30), thus likely representing a nascent (1,3;1,4)- $\beta$ -glucan produced during recombinant protein expression.

Although at lower resolution and markedly weaker than the surrounding protein map, the polymer density suggests the presence of at least six glucosyl units. Notably, the glucan starts within the catalytic pocket, at the membrane distal side of W676 of the conserved QxxRW motif. The W residue of the QxxRW motif coordinates the acceptor glucosyl unit via CH- $\pi$  stacking interactions (22, 27, 30). This suggests that the oligosaccharide copurifying with CslF6 is in a pretranslocation position, i.e., representing a state after chain

elongation yet before translocation, as also observed for bacterial CesA (30).

### CslF6 shares a conserved active site with bona fide CesAs

Compared to hybrid aspen CesA8, TM helix 7 of CslF6 is shifted by about 15 Å toward TM helices 5 and 6 (Fig. 3A). The corresponding helix in the CesA8 homotrimer interacts with TM helices 4 and 5 of a neighboring protomer, thereby contributing to oligomerization (22).

As confirmed by our biochemical analyses, CslF6 catalyzes glycosyl transfer to either the C3 or C4 hydroxyl of the accepting sugar, requiring proper acceptor positioning relative to a base catalyst. Analogous to bacterial and plant CesAs, the general base is likely formed by the aspartate (D634) of the conserved TED motif at the N terminus of a short helix directly adjacent to the acceptor binding site (30).

Superimposing the CslF6 and CesA8 structures reveals a notable conservation of the catalytic pocket, including the TED motif

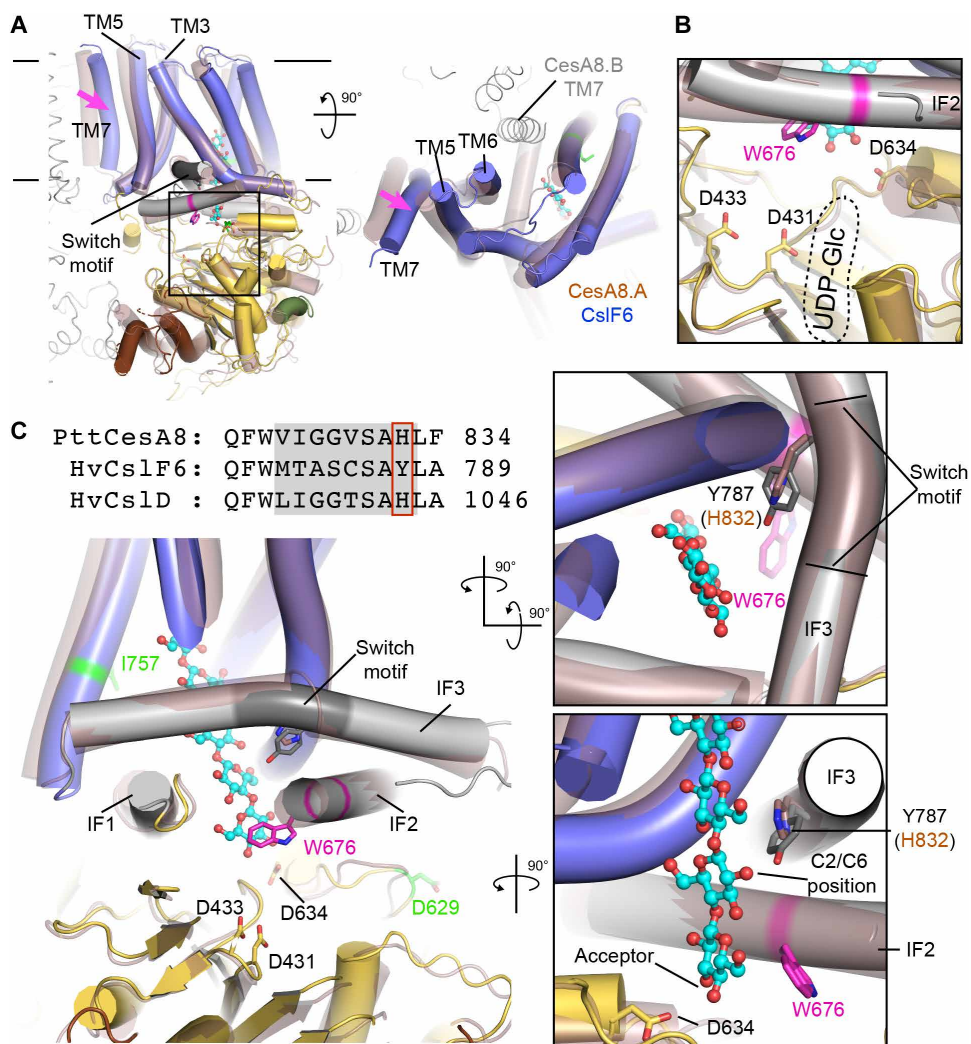


**Fig. 3. CslF6 adopts a CesA-like architecture.** (A) CslF6 was superimposed with one protomer of the hybrid aspen (Ptt) CesA8 trimeric structure (PDB: 6WLB). One CesA8 protomer is shown as a semitransparent cartoon colored dark violet, and the others are shown as gray ribbons. The nascent cellulose polymer present in PDB: 6WLB is shown as cyan and red ball and sticks in all panels. CslF6 is shown as a cartoon colored blue, gray, yellow, green, and brown for its TM, interface, GT, CSR, and PCR regions, respectively. (B) Conservation of the active site. The panel enlarges the region indicated with a black rectangle in (A). The substrate-binding pocket is indicated by a dashed oval. (C) Sequence alignment of the switch motif from hybrid aspen CesA8 and barley CslF6 and CslD and localization in the 3D structure. Hybrid aspen CesA8 is superimposed and shown as in (A).

(Fig. 3B). No additional residues or substitutions are observed that may function as base catalysts under physiological conditions or suggest an alternative substrate-binding pose. This indicates that CslF6 always binds its UDP-glucose substrate in the same conformation and uses the same base catalyst to activate the acceptor's C3 or C4 hydroxyl group.

Focusing on the cytosol-proximal region of the TM channel, we compared the primary sequences of CesAs, CslF6s, and CslDs, the latter being the most closely related Csl enzymes to CslF6 (11). Notably, this analysis revealed a sequence motif conserved among the cellulose-producing enzymes (CesAs and CslDs) that diverged in the CslF6 lineage (Fig. 3C and fig. S7). This motif, hereafter designated as “switch motif,” corresponds to the VIGGSAH sequence in CesA/CslD and MTASCSAY in CslF6 (fig. S7). It belongs to IF3 which, together with IF1, IF2, and TM helix 3, frames the cytosolic entrance to CslF6's TM channel (Fig. 2B). The CesA8 structure containing a nascent cellulose oligosaccharide reveals close proximity between the switch motif's C-terminal H832 and the

second and third glucosyl units of the nascent cellulose chain (22). This residue is a tyrosine in CslF6 (Y787) that likely extends farther into the TM channel. The side chain's hydroxyl group could form a hydrogen bond with the translocating glucan, especially at its C6 positions (Fig. 3C).

### The switch motif controls (1,3)- $\beta$ -glycosyl linkage formation

We performed single-point mutagenesis and swapping analyses (table S2) to test whether the switch motif and particularly Y787 control CslF6's ability to introduce (1,3)- $\beta$ -glucosyl linkages into the synthesized glucan. The mutant enzymes were expressed and purified as described for wild-type CslF6, with no major reduction in protein stability or catalytic activity (Fig. 4 and fig. S8).

Replacing Y787 in barley CslF6 with the corresponding H residue found in CesAs markedly reduces (1,3)- $\beta$ -linkage formation (Fig. 4, A and B). The *in vitro*-synthesized polymer is no longer degraded by lichenase or (1,3)- $\beta$ -glucan endohydrolase, while cellulase continues to hydrolyze it. Similar results were obtained with a

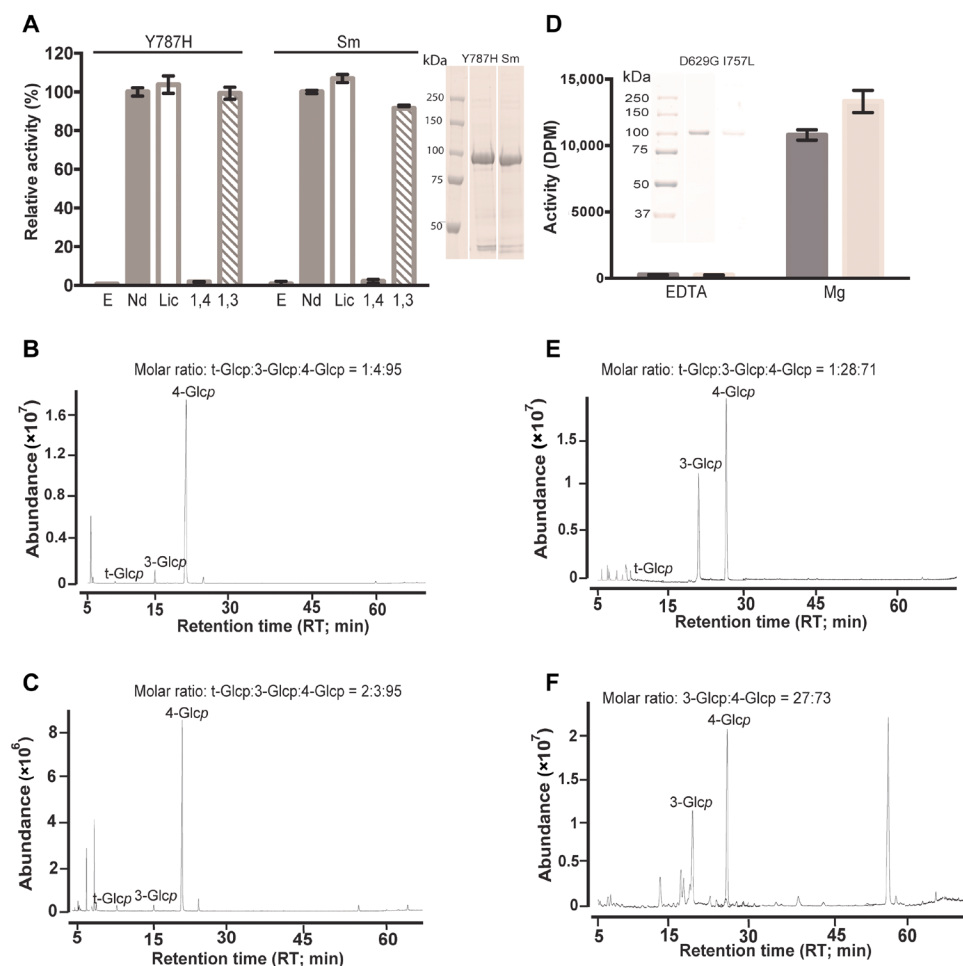


**Fig. 4. CslF6 mutagenesis affecting (1,3;1,4)- $\beta$ -glucan biosynthesis.** (A) Polysaccharide products recovered from *in vitro* synthesis reactions with the CslF6 mutants, Y787H, and Sm (CslF6 with its switch motif replaced with the corresponding IF3 region from CesA8). Reactions were performed in the presence of EDTA (E), no degrading enzymes (Nd), lichenase (Lic), and endo-(1,4)- and (1,3)- $\beta$ -glucanase (1,4 and 1,3, respectively). Product yields are normalized to undigested samples. Error bars represent SDs from three independent replicas. Inset: Coomassie-stained 7.5% SDS-PAGE of the purified mutants. (B and C) Permethylated alditol acetates obtained from linkage analyses of the polymers produced by the Y787H (B) and Sm mutants (C). (D) Catalytic activity of the D629G (dark gray) and I757L (light gray) mutants as described for the wild-type enzyme in Fig. 1. DPM, disintegrations per minute. Inset: Coomassie-stained 10% SDS-PAGE of the purified mutants. (E and F) Glycosyl linkage analyses of glucans produced by the D629G and I757L mutants.

switch motif–swapped CslF6 (denoted as “Sm”) in which the entire switch motif was replaced with the corresponding sequence of CesAs (Fig. 4, A and C). The reverse experiment, introducing the CslF6 switch motif into hybrid aspen CesA8, did not result in (1,3)- $\beta$ -linkage formation (fig. S9), suggesting that the identified switch motif is necessary but not sufficient for (1,3)- $\beta$ -glucosyl linkage formation (see Discussion).

The products of the mutant enzymes were also characterized by glycosidic linkage analyses (Fig. 4, B and C, and fig. S10). In agreement with enzymatic degradation assays, the CslF6-Y787H point mutant and switch motif–swapped Sm constructs synthesize a predominantly (1,4)-linked  $\beta$ -glucan (i.e., cellulose), with only a minor fraction of (1,3)- $\beta$ -linked glucosyl units. The apparent ratio of (1,3)- to (1,4)-linkages drops from 1:2 for the wild-type enzyme to about 1:24 and 1:32 for the single residue and switch motif–swapped constructs, respectively. These mutants appear to synthesize polysaccharides with DPs close to 100 (Fig. 4, B and C, and fig. S10). However, it should be kept in mind that the limit of detection of the GC–mass chromatography (GC–MS) approach used to estimate the DP of the polymer synthesized is around 100, which suggests that, in some cases, chain length might well exceed a DP of 100. Similar linkage analyses did not detect any (1,3)-linkages in the products of the corresponding CesA8 mutants, in agreement with the enzymatic degradation results (figs. S9 and S11).

In addition to the identified switch motif, previous site-directed mutageneses of CslF6 expressed in *Nicotiana benthamiana* identified several residues within the enzyme’s GT domain and TM region affecting the likelihood of forming (1,3)- $\beta$ -glucosyl linkages (21, 34). These include an isoleucine-to-leucine substitution within TM helix 4 and an aspartate-to-glycine replacement within the GT domain (Fig. 3C). We introduced these mutations into wild-type CslF6 (I757L and D629G) and analyzed the in vitro–synthesized glucan enzymatically and via glycosidic linkage analyses. The substitutions slightly reduce (1,3)-linkage formation by CslF6, resulting in a DP3:DP4 ratio of about 1:2.5, compared to 1:2 for the wild-type enzyme (Fig. 4, D to F, and fig. S12). However, compared to the switch motif substitutions, the observed effects are minor, and the mutants exhibit reduced overall catalytic activity (fig. S8).

## DISCUSSION

CesA-like enzymes synthesize diverse cell wall polysaccharides, including mannans (family A), xyloglucans (family C), cellulose (family D), and (1,3;1,4)- $\beta$ -glucans (families F, H, and J) (35–37). On a molecular level, the enzymes differ primarily in the length and sequence of their N-terminal domains preceding the first TM helix and the PCR and CSR. We show here that barley CslF6 is necessary and sufficient to synthesize a (1,3;1,4)- $\beta$ -glucan in vitro, confirming that the enzyme introduces (1,3)- $\beta$ -glucosyl linkages at irregular yet nonrandom positions in the otherwise (1,4)- $\beta$ -linked glucan. Biosynthesis only requires the substrate UDP-glucose and magnesium as the divalent cation.

We were unable to detect CslF6 homo-oligomerization similar to the trimerization of CesAs (22, 27, 33). Because (1,3;1,4)- $\beta$ -glucans do not form fiber-like structures comparable to cellulose, the polymeric products released from monomeric or oligomeric forms of CslF6 may not differ substantially in their material properties. Notably, CslD, which is implicated in polarized cell wall cellulose deposition, has been shown to oligomerize in vitro, perhaps similar

to bona fide CesAs (37, 38). Because CslD produces cellulose, oligomerization may be necessary to spatiotemporally orchestrate glucan secretion to form fibrillar cellulosic materials (39). Thus, we conclude that CslF6 preferentially functions as a monomer, although oligomerization in vivo mediated by other factors cannot be excluded at this stage.

CslF6 and the related cellulose, chitin, and hyaluronan synthases likely start polysaccharide biosynthesis by hydrolyzing a substrate molecule to release a priming monosaccharide (40–43). Following CslF6 priming, the initial acceptor is likely positioned with its C4 hydroxyl group toward the base catalyst to form a (1,4)- $\beta$ -linkage in a subsequent glycosyl transfer reaction (42). However, synthesizing a (1,3;1,4)- $\beta$ -glucan necessitates acceptor activation either at its C3 or C4 position (Fig. 5). The profound similarity of barley CslF6’s catalytic domain with plant and bacterial CesAs suggests the presence of a single-base catalyst only, i.e., D634 of the TED motif. Thus, introducing a (1,3)- $\beta$ -linkage into an otherwise (1,4)- $\beta$ -linked glucan requires repositioning the acceptor sugar (and, hence, its C3 or C4 hydroxyl group) by about 2 Å relative to D634.

A sequence comparison of cellulose and (1,3;1,4)- $\beta$ -glucan–synthesizing enzymes provides insights into how (1,3)- $\beta$ -linkages may be introduced. The identified switch motif lining the secretion channel is a defining sequence element of CslF6 enzymes. We postulate that it recognizes specific features of the translocating glucan (Fig. 5).

In the (1,4)- $\beta$ -glucan cellulose, neighboring glucosyl units are rotated by about 180° relative to each other. This alternating orientation is established at the active site following chain elongation and positions the C6 hydroxyl groups of consecutive glucosyl units on opposing sides of the ribbon-shaped polymer (Fig. 5). A similar alternating orientation likely occurs between adjacent (1,4)-linked glucosyl residues in a (1,3;1,4)- $\beta$ -glucan. Accordingly, register-dependent interactions of the switch motif with the nascent glucan could introduce the characteristic (1,3)- $\beta$ -linkages by repositioning the acceptor sugar at the active site.

The CslF6 structure suggests that the switch motif’s C-terminal Y787 is within hydrogen bonding distance to the C6 hydroxyl group of the polymer’s second or third glucosyl unit, following the terminal acceptor sugar. The acceptor, in turn, stacks against W676 of the QxxRW motif at the TM channel entrance, as observed in CesA. However, owing to the  $\sim$ 180° rotation of the glucan’s glucosyl units, Y787 would only interact with the C6 hydroxyl of either the second or third sugar, depending on the polymer’s register during translocation (Fig. 5, B and C).

We propose that interactions of Y787 with the C6 hydroxyl of the polymer’s penultimate glucosyl unit (counting from the non-reducing end) reposition the acceptor to favor glucosyl transfer to its C3 hydroxyl group, instead of its C4 hydroxyl (Fig. 5B). Applying this rule generates a glucan with only DP3 units upon lichenase digestion. For stereochemical reasons, the C6 hydroxyl group of a (1,4)- $\beta$ -linked glucosyl unit following a (1,3)- $\beta$ -linked unit likely points to the same side of the polymer as the preceding sugar (Fig. 5E).

We further assume that the acceptor can also be repositioned through interactions of the switch motif’s Y787 with the C6 hydroxyl of the third glucosyl unit. This is supported (i) by its location relative to the nascent glucan (Figs. 2 and 3C) and (ii) by the orientation of the corresponding His residue in plant CesA structures (22, 27). Here, the histidine is positioned about halfway between the second

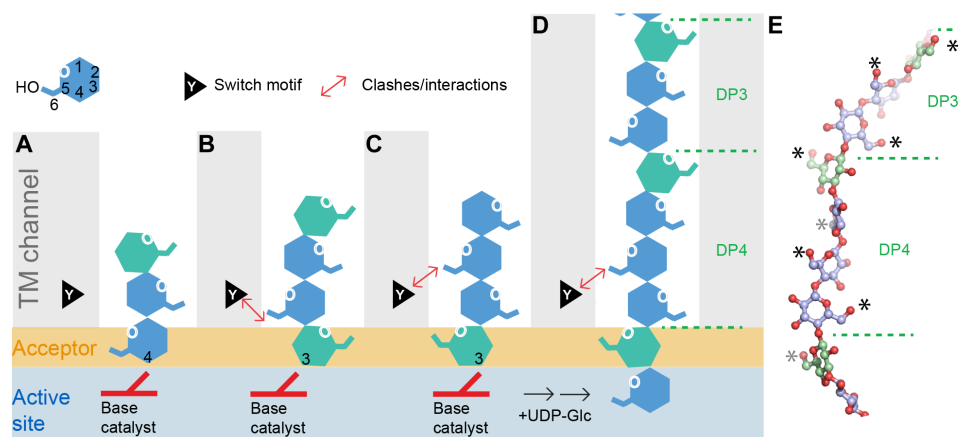


**Fig. 5. Model of (1,3;1,4)- $\beta$ -glucan biosynthesis.** (A) The C6 hydroxyl groups of consecutive (1,3)- and (1,4)- $\beta$ -linked glucosyl units point in approximately the same direction during translocation, while consecutive (1,4)- $\beta$ -linked glucosyl units are rotated by about 180°. (B) CslF6's switch motif induces acceptor repositioning due to register-dependent interactions with the penultimate glucosyl unit, resulting in the formation of DP3 segments. The position of Y787 is shown at the point of the switch motif (black triangle with a central "Y"). (C) Acceptor repositioning may also occur upon interactions with the third glucosyl unit, resulting in the formation of DP4 segments. (D) Acceptor repositioning due to interactions with the glucan's second and third glucosyl unit generates a polymer harboring DP3 and DP4 segments. (E) Model of a (1,3;1,4)- $\beta$ -glucan as shown in (D). (1,3)- and (1,4)- $\beta$ -linked glucosyl units are shown in pale green and blue for their carbon atoms, respectively. The model was generated and refined using GLYCAM ([www.glycam.org](http://www.glycam.org)), and asterisks highlight the C6 positions. Dashed lines indicate lichenase cleavage sites.

and third glucosyl unit of the nascent cellulose polymer (22, 27). In the event that Y787 is not within hydrogen bonding distance to any C6 hydroxyl group, the acceptor is likely positioned to be extended at its C4 hydroxyl group, as observed in CesaA (Fig. 5A) (22, 27). Applying these switch motif rules generates the characteristic DP3 and DP4 fragments observed upon lichenase hydrolysis (Fig. 5D). Species-dependent differences in DP3:DP4 ratios may then reflect varying probabilities of acceptor repositioning because of interactions with the glucan's second or third glucosyl unit. Although this model is consistent with our present data and agrees with previous results suggesting that residues located within CslF6's TM region influence the DP3:DP4 ratios (34), its confirmation will require high-resolution insights into CslF6-glucan translocation intermediates at different registers. Our model contrasts a recently proposed mechanism of hyaluronan synthase that introduces (1,4)- and (1,3)- $\beta$ -glycosidic linkages into a heteropolysaccharide in a substrate-dependent manner (40).

Failure to convert trimeric poplar CesaA8 to a (1,3;1,4)- $\beta$ -glucan synthase by introducing the barley CslF6 switch motif suggests that additional components are important to introduce (1,3)- $\beta$  linkages. The monomeric functional unit of CslF6, with its altered position of TM helix 7, creates a different, slightly wider TM channel. The TM architecture of (1,3;1,4)- $\beta$ -glucan synthase likely evolved to accommodate the nonlinearity of the synthesized (1,3;1,4)- $\beta$ -glucan, in contrast to the ribbon-shaped polymer synthesized by bona fide CesaAs. Notably, CslF6's IF3 contains two additional "CslF6-specific" residues N terminal to the switch motif. Here, phenylalanine and glycine residues replace conserved tryptophane and glutamate residues of the cellulose-producing enzymes (fig. S7). It is possible that these substitutions mediate channel properties in monomeric CslF6 that are also required for (1,3;1,4)- $\beta$ -glucan synthesis and translocation.

## MATERIALS AND METHODS

### Expression and purification of HvCslF6 in Sf9 insect cells

The barley CesaA-like F6 gene (*HvCslF6*) encoding an N-terminal 12xHis tag was amplified from the *HvCslF6*-pCR8 construct and

cloned into Not I and Hind III restriction sites of the baculovirus vector pACEBac1 using the primers listed (table S2). The mutants of HvCslF6 (D629G, I757L, Y787H, and Sm) and PttCesaA8 (H832Y and Sm) were generated using the mutagenesis primers listed in table S2.

Expression of HvCslF6 and its mutants was performed in Sf9 insect cells, and purification of the protein variants was carried out as previously described for the hybrid aspen [*Populus tremula*  $\times$  *tremuloides* (Ptt)] CesaA8 (21), except that 1 mM TCEP [tris(2-carboxyethyl)phosphine] instead of  $\beta$ -mercaptoethanol was used as a reducing agent in the buffer. PttCesaA8 was purified using the same procedure as for HvCslF6, but with a modified buffer system that contained 20 mM tris (pH 7.5), 100 mM NaCl, 5 mM sodium phosphate, and 5 mM sodium citrate. After gel filtration chromatography, the PttCesaA8 trimeric fractions were used for activity assays.

### Activity assays

Activity assays were performed as described (22, 27). Briefly, for the initial metal-dependent assay, 5  $\mu$ M HvCslF6 was incubated at 30°C with 5 mM UDP-glucose and 0.25  $\mu$ Ci of UDP-[ $^3$ H]-glucose in 20 mM EDTA, MgCl<sub>2</sub>, MnCl<sub>2</sub>, or CaCl<sub>2</sub> in a buffer containing 20 mM tris (pH 7.5), 0.1 M NaCl, and 1 mM TCEP. The time course of (1,3;1,4)- $\beta$ -glucan biosynthesis was monitored in different time intervals up to 24 hours. For enzymatic degradation, the in vitro product obtained after an overnight synthesis reaction was hydrolyzed with 5 U of endo-(1,3)- $\beta$ -glucosidase from *Trichoderma* sp. or endo-(1,4)- $\beta$ -glucanase from *Trichoderma longibrachiatum* or lichenase, an endo-(1,3;1,4)- $\beta$ -glucanase from *B. subtilis* (Megazyme, Wicklow, Ireland). The endoglucanases were added at the beginning of the synthesis reaction, and incubation continued overnight at 30°C. Then, the synthesis reaction was spotted onto Whatman 3MM paper and developed by descending chromatography in 60% ethanol as described (23). Following paper chromatography, the polymeric product was quantified by scintillation counting. Nonhydrolyzed samples for this analysis were treated similarly without addition of any endoglucanases.

### Pull-down assay

Coexpression of differentially tagged HvCslF6 constructs was done in *Pichia pastoris* as described earlier (22, 27). Briefly, His-, FLAG-, and Myc-tagged constructs were cloned individually into the pPICZ A *Pichia* expression vector. After transformation, the colonies were screened for coexpressing of all three CslF6 species using tag-specific antibodies for Western blotting. The positive colonies were selected for expression and pull-down assays. Protein purification was carried out as described above for Sf9 cell-expressed CslF6. After cell lysis in a microfluidizer and membrane solubilization, the membrane extract was incubated with Nickel-Nitriloacetic acid (Ni-NTA) resin for 1 hour and washed and eluted as described above, followed by Superose 6 gel filtration chromatography. Ni-NTA elution and gel filtration peak fractions were analyzed by Western blotting using anti-His, FLAG, and Myc primary antibodies and an IRDye800-coupled anti-mouse secondary antibody for detection.

### HPLC analysis of oligosaccharides derived from HvCslF6-synthesized (1,3;1,4)- $\beta$ -glucan

The in vitro (1,3;1,4)- $\beta$ -glucan polymeric product was synthesized overnight under the experimental conditions described above, except that HvCslF6 (1 mg/ml) and 10 mM UDP-glucose substrate without UDP-[<sup>3</sup>H]-glucose were used. After the synthesis, the entire reaction mixture was loaded onto a 3-kDa molecular weight cutoff (MWCO) Amicon Ultra 0.5-ml filter to remove small molecules such as excess UDP-glucose, oligosaccharides, and detergent. The retained concentrated protein and polymeric material were washed thrice with endoglucanase-specific buffers: 100 mM sodium acetate buffer (pH 4.5) for endo-1,3- $\beta$ -glucosidase and endo-1,4- $\beta$ -glucosidase and 100 mM sodium phosphate buffer (pH 6.5) for lichenase. The retained polymeric product was hydrolyzed with 5 U of each individual endoglucanase at 40°C for 3 hours. After enzymatic hydrolysis of the polymer, the mixtures were loaded again onto new 3-kDa MWCO Amicon Ultra 0.5-ml filters. This time, the filtrates containing oligosaccharide products were recovered and analyzed by HPLC.

For the control experiment, commercial barley (1,3;1,4)- $\beta$ -glucan (0.25 mg/ml; Sigma-Aldrich, St. Louis, USA) was suspended in the endo- $\beta$ -glucanase-specific buffers as described above. The polymer was hydrolyzed with each enzyme, and the oligosaccharides released were analyzed by HPLC.

The (1,3;1,4)- $\beta$ -glucan-derived oligosaccharides were separated on an Agilent 1260 Infinity II LC system (Agilent Technologies, Santa Clara, USA) on a TSKgel column G2000PW (60 cm by 7.5 mm inner diameter; TOSOH Biosciences) equilibrated with water. Oligosaccharides were eluted in water at a flow rate of 1 ml/min, and the elution was monitored using a refractive index detector. The chromatograms were compared with that of standard cellulose oligosaccharides ranging from glucose to cellobiose (Megazyme, Wicklow, Ireland).

### Glycosidic linkage analysis

Syntheses of the in vitro  $\beta$ -glucan polymer from both CslF6 and Cesa8 were performed as described above for HPLC analysis but without added hydrolytic enzymes. After overnight synthesis at 30°C, the entire mixture was precipitated with 80% (v/v) ethanol for 5 hours at room temperature (25°C). The precipitates were collected by centrifugation at 21,200g for 20 min. The pellet were washed twice with 80% (v/v) ethanol for 10 min at 21,200g and air-dried before glycosidic linkage analysis.

Glycosidic linkages were identified and quantified as described (44), with minor modifications. Briefly, 1 mg of the freeze-dried samples was methylated in anhydrous dimethyl sulfoxide by adding 0.1 ml of methyl iodide under nitrogen and sonicating for 10 min at room temperature. This step was repeated four times to avoid under-methylation of the polysaccharides. One milliliter of dichloromethane (DCM) was subsequently added to the samples, and the methylated polysaccharides were extracted by phase partitioning against deionized water. This step was repeated three times, and the resultant combined DCM phases were evaporated under a stream of nitrogen, followed by hydrolysis at 100°C for 3 hours in 1 ml of 2 M trifluoroacetic acid under nitrogen. The hydrolysates were reduced overnight at room temperature in the presence of NaBD<sub>4</sub> under nitrogen and acetylated with acetic anhydride at 100°C for 12 hours. The PMAAs were recovered by evaporating the acetic anhydride solvent under a gentle stream of nitrogen and redissolving the samples in DCM. The PMAAs were purified by partitioning against deionized water, and the DCM phase was transferred to a GC vial and analyzed on an Agilent 7890B/5977B GC-MS (Agilent Technologies, Santa Clara, USA) fitted with a VF-23ms capillary column (30 m by 0.25 mm, 0.25  $\mu$ m; Agilent Technologies, USA). Helium was used as carrier gas, and the oven temperature was programmed as follows: from 165° to 175°C at 1°C/min, from 175° to 195°C at 0.5°C/min, from 195° to 210°C at 2°C/min, and from 210°C to 250°C at 10°C/min, followed by a plateau at 250°C for 6.5 min (total run time of 68 min). The fragmentation patterns of the different PMAAs were interpreted by referring to the Complex Carbohydrate Research Center (CCRC) Spectral Database for PMAAs (<https://glygen.ccrcc.uga.edu/ccrc/specdb/ms/pmaa/pframe.html>).

### Cryo-grids preparation

The quality of the purified HvCslF6 protein was checked by negative staining. Immediately after gel filtration chromatography, 4  $\mu$ l of protein at 0.01 mg/ml was applied to a carbon/formvar grid, followed by two washes with 4  $\mu$ l of H<sub>2</sub>O and staining with 4  $\mu$ l of 0.75% uranyl formate. The negatively stained grids were checked on a Fei Tecnai F20 at the Macromolecular Electron Microscopy Core (MEMC) facility at the University of Virginia. The remaining sample corresponding to the selected protein preparation was concentrated to ~3 mg/ml and applied (2.5  $\mu$ l) to a C-flat 300-mesh 1.2/1.3 copper grid (Electron Microscopy Sciences) glow-discharged in the presence of amylamine at 25 mA for 45 s. The grid was blotted with a Vitrobot Mark IV (FEI, Thermo Fisher Scientific, Waltham, USA) with force 7 for 12 to 14 s at 4°C, 100% humidity, frozen in liquid ethane, and stored in liquid nitrogen.

### Cryo-EM data collection

The cryo grids were screened on a Fei Titan Krios microscope operated at 300 keV and equipped with a Gatan K3 direct electron detector positioned post a Gatan Quantum energy filter at the MEMC at the University of Virginia. Datasets were collected at the Pacific Northwest Center for Cryo-EM (PNCC) on a Titan Krios microscope operated at 300 keV and equipped with a Gatan K3 direct electron detector positioned post a Gatan Quantum energy filter. Movies (6528) with 50 frames were collected from one grid with a pixel size of 0.83 Å, defocus of -2.0 to -1  $\mu$ m, and step size of 0.2  $\mu$ m. The total dose was 53 e<sup>-</sup>/Å<sup>2</sup>.

### Data processing

The cryo-EM images were processed in CryoSPARC 2.12.4 (25). Movies were corrected for full frame and sample deformation using

Patch Motion Correction followed by full-frame Contrast Transfer Function (CTF) estimation. After CTF estimation, micrographs were curated on the basis of estimated resolution (0 to 4.0 Å), drift (0 to 30 pixel), astigmatism (0 to 1000 Å), and defocus (0 to -3.0 μm) and were manually inspected for outliers and ice contamination.

Particles were automatically picked using CryoSPARC's "Blob Picker" with minimum and maximum particle diameters of 80 and 300 Å, respectively, extracted at a box size of 400 pixels, followed by 2D classification. Good class averages with different views were selected for template-based particle picking using a diameter of 300 Å and a minimum separation distance of 150 Å (0.5 × particle diameter). The particles were extracted and Fourier-cropped to a box size of 100 pixels followed by several rounds of 2D classification with 100 to 50 classes each and a batch size of 300 per class.

An initial model was built in CryoSPARC followed by 3D sorting. Particles belonging to the best class were re-extracted at a physical pixel size of 0.83 Å and 300 pixel box size followed by nonuniform refinement, yielding a density map with an estimated resolution of 5.5 Å based on Fourier Shell Correlation (FSC). Local refinement using a mask covering only the protein part improved the density quality substantially and yielded a map with an estimated resolution of 4.0 Å based on FSC. This map was used for model building.

The CslF6 model was built using an AlphaFold2-generated template and manually corrected in Coot (45) and refined in Phenix:refine (table S1) (46). Coordinates and EM maps have been deposited at the Protein Data Bank (PDB) and EM DataBank (EMDB) under accession codes 8DQK and 27655, respectively.

## SUPPLEMENTARY MATERIALS

Supplementary material for this article is available at <https://science.org/doi/10.1126/sciadv.add1596>

[View/request a protocol for this paper from Bio-protocol.](#)

## REFERENCES AND NOTES

1. K. Keegstra, Plant cell walls. *Plant Physiol.* **154**, 483–486 (2010).
2. R. G. Staudte, J. R. Woodward, G. B. Fincher, B. A. Stone, Water-soluble (1→3), (1→4)-β-D-glucans from barley (*Hordeum vulgare*) endosperm. III. Distribution of cellotriosyl and cellotetraosyl residues. *Carbohydr. Polym.* **3**, 299–312 (1983).
3. G. S. Buliga, D. A. Brant, G. B. Fincher, The sequence statistics and solution conformation of a barley (1→3, 1→4)-β-D-glucan. *Carbohydr. Res.* **157**, 139–156 (1986).
4. C. S. Brennan, L. J. Cleary, The potential use of cereal (1→3, 1→4)-β-D-glucans as functional food ingredients. *J. Cereal. Sci.* **42**, 1–13 (2005).
5. H. Collins, R. Burton, D. Topping, M.-L. Liao, A. Bacic, G. Fincher, REVIEW: Variability in fine structures of noncellulosic cell wall polysaccharides from cereal grains: Potential importance in human health and nutrition. *Cereal. Chem.* **87**, 272–282 (2010).
6. A. Lazaridou, C. G. Biliaderis, Molecular aspects of cereal β-glucan functionality: Physical properties, technological applications and physiological effects. *J. Cereal. Sci.* **46**, 101–118 (2007).
7. M. A. Anderson, B. A. Stone, A new substrate for investigating the specificity of β-glucan hydrolases. *FEBS Lett.* **52**, 202–207 (1975).
8. V. Lombard, H. G. Ramulu, E. Drula, P. M. Coutinho, B. Henrissat, The carbohydrate-active enzymes database (CAZY) in 2013. *Nucleic Acids Res.* **42**, D490–D495 (2014).
9. J. L. Morgan, J. T. McNamara, M. Fischer, J. Rich, H. M. Chen, S. G. Withers, J. Zimmer, Observing cellulose biosynthesis and membrane translocation in crystallo. *Nature* **531**, 329–334 (2016).
10. L. L. Lairson, B. Henrissat, G. J. Davies, S. G. Withers, Glycosyltransferases: Structures, functions, and mechanisms. *Annu. Rev. Biochem.* **77**, 521–555 (2008).
11. A. Little, J. G. Schwerdt, N. J. Shirley, S. F. Khor, K. Neumann, L. A. O'Donovan, J. Lahnstein, H. M. Collins, M. Henderson, G. B. Fincher, R. A. Burton, Revised phylogeny of the cellulose synthase gene superfamily: Insights into cell wall evolution. *Plant Physiol.* **177**, 1124–1141 (2018).
12. R. A. Burton, S. M. Wilson, M. Hrmova, A. J. Harvey, N. J. Shirley, A. Medhurst, B. A. Stone, E. J. Newbigin, A. Bacic, G. B. Fincher, Cellulose synthase-like CslF genes mediate the synthesis of cell wall (1,3;1,4)-beta-D-glucans. *Science* **311**, 1940–1942 (2006).
13. M. S. Doblin, F. A. Pettolino, S. M. Wilson, R. Campbell, R. A. Burton, G. B. Fincher, E. Newbigin, A. Bacic, A barley cellulose synthase-like CSLH gene mediates (1,3;1,4)-beta-D-glucan synthesis in transgenic Arabidopsis. *Proc. Natl. Acad. Sci. U.S.A.* **106**, 5996–6001 (2009).
14. S. P. Hazen, J. S. Scott-Craig, J. D. Walton, Cellulose synthase-like genes of rice. *Plant Physiol.* **128**, 336–340 (2002).
15. J. G. Schwerdt, K. MacKenzie, F. Wright, D. Oehme, J. M. Wagner, A. J. Harvey, N. J. Shirley, R. A. Burton, M. Schreiber, C. Halpin, J. Zimmer, D. F. Marshall, R. Waugh, G. B. Fincher, Evolutionary dynamics of the cellulose synthase gene superfamily in grasses. *Plant Physiol.* **168**, 968–983 (2015).
16. Y. Yin, M. A. Johns, H. Cao, M. Rupani, A survey of plant and algal genomes and transcriptomes reveals new insights into the evolution and function of the cellulose synthase superfamily. *BMC Genomics* **15**, 260 (2014).
17. C. M. Kim, S. H. Park, B. Il Je, S. H. Park, S. J. Park, H. L. Piao, M. Y. Eun, L. Dolan, C. D. Han, OsCSLD1, a cellulose synthase-like D1 gene, is required for root hair morphogenesis in rice. *Plant Physiol.* **143**, 1220–1230 (2007).
18. A. J. Bernal, C. M. Yoo, M. Mutwil, J. K. Jensen, G. Hou, C. Blaukopf, I. Sorensen, E. B. Blancaflor, H. V. Scheller, W. G. T. Willats, Functional analysis of the cellulose synthase-like genes CSLD1, CSLD2, and CSLD4 in tip-growing arabidopsis cells. *Plant Physiol.* **148**, 1238–1253 (2008).
19. S. J. Kim, S. Zemelis, K. Keegstra, F. Brandizzi, The cytoplasmic localization of the catalytic site of CSLF6 supports a channeling model for the biosynthesis of mixed-linkage glucan. *Plant J.* **81**, 537–547 (2015).
20. R. A. Burton, M. J. Gidley, G. B. Fincher, Heterogeneity in the chemistry, structure and function of plant cell walls. *Nat. Chem. Biol.* **6**, 724–732 (2010).
21. G. Dimitroff, A. Little, J. Lahnstein, J. G. Schwerdt, V. Srivastava, V. Bulone, R. A. Burton, G. B. Fincher, (1,3;1,4)-beta-Glucan biosynthesis by the CSLF6 enzyme: Position and flexibility of catalytic residues influence product fine structure. *Biochemistry* **55**, 2054–2061 (2016).
22. P. Purushotham, R. Ho, J. Zimmer, Architecture of a catalytically active homotrimeric plant cellulose synthase complex. *Science* **369**, 1089–1094 (2020).
23. P. Purushotham, S. H. Cho, S. M. Diaz-Moreno, M. Kumar, B. T. Nixon, V. Bulone, J. Zimmer, A single heterologously expressed plant cellulose synthase isoform is sufficient for cellulose microfibril formation in vitro. *Proc. Natl. Acad. Sci. U.S.A.* **113**, 11360–11365 (2016).
24. L.-I. Fu, Z.-r. Xu, J.-b. Shuai, C.-x. Hu, W. Dai, W.-f. Li, High-level secretion of a chimeric thermostable lichenase from *Bacillus subtilis* by screening of site-mutated signal peptides with structural alterations. *Curr. Microbiol.* **56**, 287–292 (2008).
25. A. Punjani, J. L. Rubinstein, D. J. Fleet, M. A. Brubaker, cryoSPARC: Algorithms for rapid unsupervised cryo-EM structure determination. *Nat. Methods* **14**, 290–296 (2017).
26. S. H. W. Scheres, RELION: Implementation of a Bayesian approach to cryo-EM structure determination. *J. Struct. Biol.* **180**, 519–530 (2012).
27. X. Zhang, Y. Xue, Z. Guan, C. Zhou, Y. Nie, S. Men, Q. Wang, C. Shen, D. Zhang, S. Jin, L. Tu, P. Yin, X. Zhang, Structural insights into homotrimeric assembly of cellulose synthase CesA7 from *Gossypium hirsutum*. *Plant Biotechnol. J.* **19**, 1579–1587 (2021).
28. J. Jumper, R. Evans, A. Pritzel, T. Green, M. Figurnov, O. Ronneberger, K. Tunyasuvunakool, R. Bates, A. Zidek, A. Potapenko, A. Bridgland, C. Meyer, S. A. A. Kohli, A. J. Ballard, A. Cowie, B. Romera-Paredes, S. Nikolov, R. Jain, J. Adler, T. Back, S. Petersen, D. Reiman, E. Clancy, M. Zielinski, M. Steinegger, M. Pacholska, T. Berghammer, S. Bodenstein, D. Silver, O. Vinyals, A. W. Senior, K. Kavukcuoglu, P. Kohli, D. Hassabis, Highly accurate protein structure prediction with AlphaFold. *Nature* **596**, 583–589 (2021).
29. K. Tunyasuvunakool, J. Adler, Z. Wu, T. Green, M. Zielinski, A. Zidek, A. Bridgland, A. Cowie, C. Meyer, A. Laydon, S. Velankar, G. J. Kleywegt, A. Bateman, R. Evans, A. Pritzel, M. Figurnov, O. Ronneberger, R. Bates, S. A. A. Kohli, A. Potapenko, A. J. Ballard, B. Romera-Paredes, S. Nikolov, R. Jain, E. Clancy, D. Reiman, S. Petersen, A. W. Senior, K. Kavukcuoglu, E. Birney, P. Kohli, J. Jumper, D. Hassabis, Highly accurate protein structure prediction for the human proteome. *Nature* **596**, 590–596 (2021).
30. J. Morgan, J. Strumillo, J. Zimmer, Crystallographic snapshot of cellulose synthesis and membrane translocation. *Nature* **493**, 181–186 (2013).
31. C. E. Vergara, N. C. Carpita, β-D-Glycan synthases and the CesA gene family: Lessons to be learned from the mixed-linkage (1→3), (1→4)β-D-glucan synthase. *Plant Mol. Biol.* **47**, 145–160 (2001).
32. P. S. Rushton, A. T. Olek, L. Makowski, J. Badger, C. N. Steussy, N. C. Carpita, C. V. Stauffacher, Rice cellulose synthaseA8 plant-conserved region is a coiled-coil at the catalytic core entrance. *Plant Physiol.* **173**, 482–494 (2017).
33. T. R. Scavuzzo-Duggan, A. M. Chaves, A. Singh, L. Sethaphong, E. Slabaugh, Y. G. Yingling, C. H. Haigler, A. W. Roberts, Cellulose synthase 'class specific regions' are intrinsically disordered and functionally undifferentiated. *J. Integr. Plant Biol.* **60**, 481–497 (2018).
34. S. A. Jobling, Membrane pore architecture of the CslF6 protein controls (1,3;1,4)-β-glucan structure. *Sci. Adv.* **1**, e1500069 (2015).
35. M. Pauly, S. Gille, L. Liu, N. Mansoori, A. de Souza, A. Schultink, G. Xiong, Hemicellulose biosynthesis. *Planta* **238**, 627–642 (2013).

36. A. H. Liepman, D. M. Cavalier, The CELLULOSE SYNTHASE-LIKE A and CELLULOSE SYNTHASE-LIKE C families: Recent advances and future perspectives. *Front. Plant Sci.* **3**, 109 (2012).
37. J. Yang, G. Bak, T. Burgin, W. J. Barnes, H. B. Mayes, M. J. Pena, B. R. Urbanowicz, E. Nielsen, Cellulose synthase-like D (CSLD) 3 protein is a beta-1,4-glucan synthase. *Plant Cell* **32**, 1749–1767 (2020).
38. J. Yang, G. Bak, T. Burgin, W. J. Barnes, H. B. Mayes, M. J. Pena, B. R. Urbanowicz, E. Nielsen, Biochemical and genetic analysis identify CSLD3 as a  $\beta$ -1,4-glucan synthase that functions during plant cell wall synthesis. *Plant Cell* **32**, 1749–1767 (2020).
39. H. Yang, J. D. Kubicki, A density functional theory study on the shape of the primary cellulose microfibril in plants: Effects of C6 exocyclic group conformation and H-bonding. *Cellul.* **27**, 2389–2402 (2020).
40. F. P. Maloney, J. Kuklewicz, R. A. Corey, Y. C. Bi, R. Y. Ho, L. Mateusiak, E. Pardon, J. Steyaert, P. J. Stansfeld, J. Zimmer, Structure, substrate recognition and initiation of hyaluronan synthase. *Nature* **604**, 195–201 (2022).
41. P. Orlean, D. Funai, Priming and elongation of chitin chains: Implications for chitin synthase mechanism. *Cell surface (Amsterdam, Netherlands)* **5**, 100017 (2019).
42. J. L. W. Morgan, J. T. McNamara, J. Zimmer, Mechanism of activation of bacterial cellulose synthase by cyclic di-GMP. *Nat. Struct. Mol. Biol.* **21**, 489–496 (2014).
43. J. McManus, H. Yang, L. Wilson, J. Kubicki, M. Tien, Initiation, elongation, and termination of bacterial cellulose synthesis. *ACS Omega* **3**, 2690–2698 (2018).
44. F. A. Pettolino, C. Walsh, G. B. Fincher, A. Bacic, Determining the polysaccharide composition of plant cell walls. *Nat. Protoc.* **7**, 1590–1607 (2012).
45. P. Emsley, K. Cowtan, Coot: Model-building tools for molecular graphics. *Acta Crystallogr. D Biol. Crystallogr.* **60**, 2126–2132 (2004).
46. P. V. Afonine, R. W. Grosse-Kunstleve, N. Echols, J. J. Headd, N. W. Moriarty, M. Mustyakimov, T. C. Terwilliger, A. Urzhumtsev, P. H. Zwart, P. D. Adams, Towards automated crystallographic structure refinement with phenix.refine. *Acta Crystallogr. D Biol. Crystallogr.* **68**, 352–367 (2012).
47. R. C. Edgar, MUSCLE: Multiple sequence alignment with high accuracy and high throughput. *Nucl. Acid Res.* **32**, 1792–1797 (2004).
48. A. M. Waterhouse, J. B. Procter, D. M. Martin, M. Clamp, G. J. Barton, Jalview version 2—A multiple sequence alignment editor and analysis workbench. *Bioinformatics* **25**, 1189–1191 (2009).

**Acknowledgments:** We thank C. Lopez and J. Myers at the PNCC and K. Dryden and M. Purdy at the University of Virginia's MEMC for assistance in data collection. **Funding:** PNCC at OSHY was supported by NIH grant U24GM129547. Data were accessed through EMSL (grid.436923.9), a DOE Office of Science User Facility sponsored by the Office of Biological and Environmental Research. MEMC is funded by an NIH Recovery grant (1G20RR31199). The MEMC Titan Krios and Gatan K3/GIF detector were funded through the NIH (grants SIG S10-RR025067 and U24-GM116790, respectively). P.P., R.H., and J.Z. were supported by the Center for Lignocellulose Structure and Formation, an Energy Frontier Research Center funded by the U.S. Department of Energy, Office of Science, Basic Energy Sciences (award DESC0001090). We are also grateful for support from the Australian Research Council's (ARC) Centre of Excellence in Plant Cell Walls (grant no. CE1101007). L.Y. was supported by Adelaide Glycomics via an ARC Discovery Project grant to V.B. (grant no. DP180103974). J.Z. is a Howard Hughes Medical Institute Investigator. **Author contributions:** P.P. expressed, purified, and biochemically characterized the enzyme. P.P. and R.H. prepared cryo-EM grids. R.H. collected and processed the cryo-EM data. L.Y. performed all glycosyl linkage analyses. V.B. and G.B.F. contributed to data analyses and writing of the manuscript. All authors analyzed and interpreted the data. J.Z., V.B., and G.B.F. wrote the initial manuscript, and all authors edited the manuscript. **Competing interests:** P.P. and J.Z. are inventors on a pending patent application. The authors declare that they have no other competing interests. **Data and materials availability:** All data needed to evaluate the conclusions in the paper are present in the paper and/or the Supplementary Materials. Protein coordinates and the corresponding EM map have been deposited at the PDB/EMDB under accession codes 8DQK/27655.

Submitted 24 May 2022  
Accepted 26 September 2022  
Published 11 November 2022  
10.1126/sciadv.add1596